Journal of Physics D: Applied Physics

The early days of high-resolution X-ray topography

To cite this article: A R Lang 1993 *J. Phys. D: Appl. Phys.* **26** A1

View the article online for updates and enhancements.

You may also like

- Imaging nanoscale lattice variations by machine learning of x-ray diffraction microscopy data
Nouamane Laanait, Zhan Zhang and Christian M Schlepütz
- Identifying dislocations and stacking faults in GaN films by scanning transmission electron microscopy
X J Su, M T Niu, X H Zeng et al.
- Dislocation-induced stress in polycrystalline materials: mesoscopic simulations in the dislocation density formalism
D V Berkov and N L Gorn

Recent citations

- Dynamic observation of dislocation evolution and interaction with twin boundaries in silicon crystal growth using in – situ synchrotron X-ray diffraction imaging
M.G. Tsoutsouva *et al*
- X-Ray Diffraction Topography Methods (Review)
V. V. Lider
- X-Ray Topography-More than Nice Pictures
Andreas N. Danilewsky

This content was downloaded from IP address 202.122.36.44 on 14/12/2021 at 02:28

J. Phys. D: Appl. Phys. 26 (1993) A1–A8. Printed in the UK

The early days of high-resolution x-ray topography

A R Lang

H H Wills Physics Laboratory, University of Bristol, Tyndall Avenue, Bristol BS8 1TL, UK

Abstract. Images of the surface or interior of a single crystal formed by x-rays Bragg-reflected from its lattice planes provide information about lattice misorientations and defects in a unique way that was appreciated by the pioneers of topographic techniques: Berg, Barrett, Guinier, Ramachandran and Wooster. High-resolution images were achieved when use of fine-grain photographic emulsions was combined with diffraction geometries, providing micrometre-scale geometrical resolution. The detection of individual dislocations by x-ray diffraction contrast was reported in 1958 by three laboratories independently, employing quite different diffraction geometries. The value of x-ray diffraction contrast as a method of general application in detecting and identifying lattice defects (as opposed to special methods such as chemical etching) was demonstrated principally by the geometrically simply interpretable images of the projection topograph. Within a few months in 1958 this technique showed how dislocation Burgers vectors could be determined, how stereo-pairs of images could be formed, and how structure amplitudes could be measured absolutely from Pendellösung fringes in images of wedge-shaped crystals (though it was the hook-shaped Pendellösung fringe patterns appearing in section topographs that led Kato to develop his spherical-wave diffraction theory). The 'failure of Friedel's Law' revealed on early stereo-pairs of dislocation images suggested that *sense* as well as *direction* of Burgers vectors could be determined: confirmation came from the experiments of Hart applying the 'refraction of energy-flow' theory of Penning and Polder. X-ray topographic imaging by Polcarová and Lang of internal magnetic domain structures on the scale of a few micrometres in Fe–Si (magnetostriction constant 2.7×10^{-5}) confirmed the high strain-sensitivity of the method and its ability to explore phenomena not accessible by other investigative techniques.

1. Background

This paper covers the first five years of high-resolution x-ray topography, taken as the period 1957–62. To understand the underlying motivation and methods it is necessary to go back a decade earlier. The considerable variety of x-ray topographic techniques that have appeared in the last half century can be judged from a recent review (Lang 1992). Here there is only space to recall one route into x-ray topographic country, which will be the author's own. The story is told most easily using the first person, and that procedure is adopted (with apology for apparent egocentricity).

There was much interest in crystal texture at the Cavendish Laboratory, Cambridge, when I went there in late 1947 to work with W A Wooster and G N Ramachandran. The latter had already coined the term 'x-ray topograph' (Ramachandran 1944), and the Woosters also devised a topographic technique (Wooster and Wooster 1945). Moreover, there were two people around who well understood the dynamical theory of x-ray diffraction, Hirsch and Ramachandran; and they wrote papers of lasting practical use (Hirsch and Ramachandran 1950, Hirsch 1952). After my year with Wooster and Ramachandran I turned to instrumentation developments, which included a diffractometer, an x-ray proportional counter design optimized for x-ray diffractometry, and methods of diffracted-beam monochromatization. In the latter context all methods of crystal perfection assessment were relevant, but I was interested particularly in x-ray transmission methods and the possibility of using plastically deformed Al single crystals as focusing monochromators. The assessment methods of Guinier and Tennevin (1949) appealed. (Their white-radiation methods, like that of Ramachandran, have come back to life in everyday use for synchrotron radiation topography.)

In 1951 I proposed to my colleagues that information on relative phases should be obtainable from the fine structure at Kossel cone intersections, i.e. under conditions when two non-parallel Bragg planes simultaneously diffract. Ten years later this aim was realized, using the topographic technique under 'three-beam conditions' (see section 8).

0022-3727/93/0400A1+08$07.50 © 1993 IOP Publishing Ltd

After Cambridge I went to the USA to work at Philips Laboratories, Irvington-on-Hudson, New York, landing in New York on 24 April 1952. Towards the end of 1953 the choice between two quite different openings presented itself, to go to Caltech to work with Linus Pauling on protein structures, or to join Bruce Chalmers at Harvard where he was setting up a physical metallurgy group. I consulted Ewald for advice. He said drily 'Don't ask me: I can tell from your voice that you have made up your mind'. I went to Harvard and started to grow metal single crystals myself.

2. Preparations

Single crystals of tin and lead can be grown unenclosed in graphite boats so that the advancing solidification front can be closely observed. Theory, techniques and fascinating phenomena associated with growth from the melt are described by Chalmers (1964). One watched the crystal growing apparently perfectly at first, then developing a lineage structure (see figures 2.19 and 4.2 in Chalmers' book), the misorientations becoming specularly detectable. Where did the dislocations come from and how did they come together to form the low-angle boundaries? One would like to see *into* the crystal to find out. Tin and lead were too strongly absorbing to be penetrated in several millimetre thickness by the x-ray energies we had available, but aluminium was not. The section topograph, with several variants (Lang 1957a) was applied first to Al and LiF crystals. For such x-ray experiments an early model Hilger Microfocus tube (projected focus size about 30 μm by 3 μm, but maximum tube current only 300 μA) was obtained on loan. With the good geometrical resolution it made possible, and with tight control of diffraction conditions, the fine-scale diffraction geometry associated with Umweganregungen and Aufhellungen production could be demonstrated and clarified (Lang 1957b). But lacking even a Geiger counter, I had to find my diffracted beams by close viewing of a fluorescent screen after a half-hour wait in total darkness in order to gain sufficient dark adaptation. I set about designing a robust but precise diffractometer that would fulfil both immediate and foreseeable needs. It had independent theta and two-theta rotations settable to 1″, a linear traversing mechanism for step-wise or continuous to-and-fro translation of the specimen, stationary-film and moving-film facilities. Moreover, it was designed for easy adjustment in conditions of near darkness, which ensured its 'user-friendliness' under standard lighting. Sadly, the drawings of it remained neatly rolled up for many months until I obtained funds from the National Science Foundation for its construction. It was ready just in time for taking scanning reflection topographs which were shown at the Fourth IUCr Congress in Montreal, July 1957 (Lang 1957c). Some of the accessories designed and constructed then have only been occasionally used, but I have never found need to add to or modify a single feature in the original design. That is the 'Lang camera' that I use today.

3. Seeing individual dislocations

From what was known by the mid-1950s from etch-pit studies of dislocation densities within the subgrains in crystals such as LiF, which I could examine by section topography, and other species I examined in reflection, I concluded that statistical fluctuations in local dislocation density should produce detectable local variations in integrated reflection, and these I observed. In this period there was competition between laboratories as to who could grow Si or Ge with the lowest dislocation density; the figure was continuously coming down: 10^6, 10^4, 10^2 lines/cm^2, till W C Dash grew silicon nearly dislocation free. I was stupidly diffident about approaching the silicon-growers for specimens to examine with my x-ray technique. With fine-grain x-ray films I could have well resolved individual dislocation images at densities of 10^4 lines/cm^2 or more. The time gap between seeing individual dislocations by TEM and by x-ray diffraction contrast could have been much less, possibly zero! My first silicon specimens, supplied by Bill Dash, were already of very low dislocation density and I started taking section topographs of them immediately after the Montreal Congress. They were too thick to give clear images with a crystal traversing technique, but on the section topographs the intersection of the dislocation line by the ribbon incident beam was marked by a dot of very intense reflectivity, the 'direct' or 'kinematic' image, whereas the rest of the dislocation line within the Borrmann triangle produced a complex 'extinction shadow'. (That was the term I used. Later it became known as the 'dynamical' image.) From stepping sequences of section topographs I constructed maps of the fairly curvilinear trajectories of the few grown-in dislocations in Dash's crystals, and sent the crystals back to Bill Dash to compare with what he saw under the infrared microscope after decorating the dislocations by copper precipitates. Unfortunately, the night these precious specimens were put in the furnace for diffusing-in copper on to the dislocations the furnace control failed. The specimens overheated and copper was everywhere in them. By that time I was away from my laboratory and had no chance to repeat a comparison between infrared microscopy and x-ray topography until the end of September 1957. I myself had no doubt that individual dislocations were being seen by x-ray diffraction contrast, and I scolded myself for not earlier making the 'back of the envelope' calculation that explained why with short wavelengths such as AgKα the narrow angular reflection width $\Delta\theta_B$ of a perfect silicon crystal caused the volume surrounding the dislocation in which lattice tilt exceeded $\Delta\theta_B$, when $g \cdot b \neq 0$, to be up to 20 μm in diameter, and able to diffract kinematically, producing a spot of high integrated reflection on the image.

The published comparison with infrared micrographs (Lang 1958) was made with the help of J R Patel. The specimen was rather thick (3 mm) but I found an array of dislocations not far from the x-ray exit surface whose extinction shadows across the base of the Borrmann triangle in a section topograph gave

a two-dimensional pattern of their trajectories directly comparable with the infrared picture. When Jim Patel supplied me with crystal slices not more than 1 mm thick I could use my projection topograph technique (Lang 1959) for dislocation mapping. Several different ways of seeing individual dislocations by x-ray diffraction contrast were published in 1958, by workers operating quite independently. Jack Newkirk (1958) used the Berg–Barrett method, Borrmann, Hartwig and Irmler (1958) saw the 'deficiency' contrast of dislocations under conditions of strong anomalous transmission, and Bonse and Kappler (1958) recorded the strain fields at dislocation outcrops using the double-crystal topograph technique pioneered by Bond and Andrus (1952). The geometrically easily interpretable dislocation patterns, the strong positive diffraction contrast (under low or fairly low absorption conditions), the convenience for producing topographs with different diffraction vectors, and above all, the ability to image crystal *interiors*, put my projection topograph technique in the best position (in my view) for exploiting this new, non-destructive means of rendering dislocations visible.

4. Pendellösung

The standard treatment of diffraction by perfect crystals considered either the Bragg case, involving reflection by crystals of infinite lateral extent, or the Laue case, involving transmission by crystals of infinite lateral extent. These did not help me directly towards predicting the intensity profile from perfect whisker crystals that were cylinders or prisms in cross section. In an early morning walk across the campus of the University of Maryland in 1956 I put this dilemma before Professor Ryozi Uyeda of Nagoya. (We were attending the Electron Physics Conference in Washington, DC.) 'Do you know anyone who can tackle this problem', I said. He answered 'Indeed yes, I have a good student, Norio Kato, who has solved the problem of diffraction by a polyhedral crystal in the electron case'. I was fortunate in being able to invite Kato to join me at Harvard. (Another happy outcome of my meeting with Uyeda is also included in his recollections (Uyeda 1981).)

A few weeks after the experiments described in section 3, I was taking projection topographs of D-shaped slices of silicon provided by Jim Patel. They were cut parallel to planes making 70.5° with the [111]-type growth axis of the crystals, as shown in figure 1. The curved edge of the crystal was a wedge. In the projection topographs of such wedges fringes appeared parallel to wedge thickness contours (figure 2). They were clearly not due to the dislocations or any crystal defect, or any experimental artefact, but were a genuine diffraction effect. Kato had just arrived and I showed him the fringes, saying 'They remind me of a diagram (figure 3, from Ewald (1933)) I have seen in one of Ewald's papers, but I don't understand the theory at all'. Kato replied 'It is the Pendellösung phenomenon! Moreover, with known wavelength, wedge angle, and diffraction angles we can

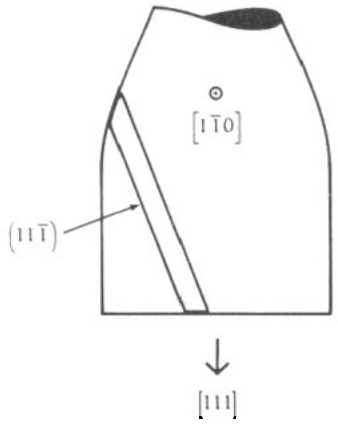

Figure 1. Geometry of $(11\bar{1})$ slice cut from a silicon crystal with [111] growth axis.

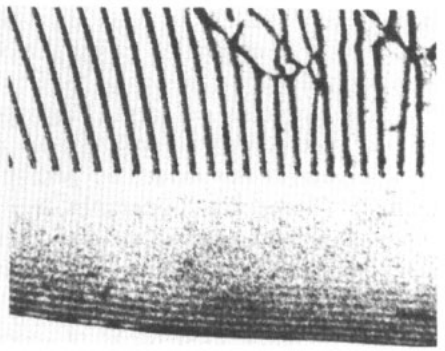

Figure 2. Projection topograph of part of wedge edge of $(11\bar{1})$ slice of silicon. Field corresponds to bottom right corner of figures 4(*a*)–(*d*). Field width 1.4 mm. Radiation AgKα_1, 022 reflection. (Note bimodal intensity profile across dislocation images in top half of field.)

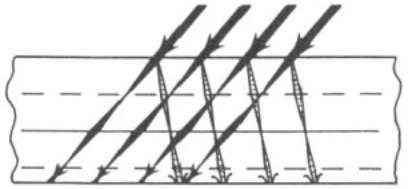

Figure 3. Ewald's diagram of Pendellösung in the Laue case.

calculate the structure amplitude directly from the Pendellösung fringe spacing!' This idea of measuring $|F|$ *absolutely* by measuring fringe spacings rather than by absolute intensity measurements, with all their manifold difficulties, was highly attractive. How this research developed is well known, and Kato's own account has now been written (Kato 1992).

The projection topograph images of the Pendellösung fringes looked simple, but the section topograph images, with their hook-shaped fringes, raised problems (Kato and Lang 1959). I did not at that time perceive the theoretical subtleties (and my efforts were all directed towards taking pictures of dislocations), but Kato did, and set about developing his 'spherical wave theory' that solved the problems so elegantly.

5. Dislocation reactions

As well as having my versatile topograph camera to facilitate experiments, I now had scintillation counters and a standard-strength x-ray generator (long focus-to-specimen distance, and shortest specimen-to-emulsion distance kept geometrical resolution good). Indeed the combination of the three factors—the camera, well-controlled, 'clean' x-ray beams and use of fine-grain, high halide-density nuclear emulsions—ensured rapid progress in the winter of 1957–8. Weeks rather than months saw the development of the hkl, $\bar{h}\bar{k}\bar{l}$ stereo-pair technique, the establishment of dislocation visibility rules (which were similar to those applying in TEM), and observation of phenomena such as bimodal intensity maxima in dislocation images (as seen in figure 2), the 'failure of Friedel's Law' (dealt with in section 7), fault surfaces and decorated dislocations in natural quartz crystals, etc. Matters such as the verification of Frank's rule of the conservation of Burgers vector at dislocation nodes and manifestations of the Lomer reaction between dislocations on different (111)-type planes (Lomer 1951) all seemed so natural that no pause to publish the observations was made. So perhaps now is an opportunity to show some topographs, well over 30 years old, that demonstrate more striking occurrences of individual Lomer reactions than were described later (Jenkinson and Lang 1962).

Figures 4(*a*)–(*d*) show topographs of more of the 1 mm thick, *D*-shaped slice of silicon cut parallel to $(11\bar{1})$ from a crystal with [111] growth axis (according to the geometry explained in figure 1), part of whose wedge-shaped periphery was shown in figure 2. To understand the variations in dislocation visibility, recall the following rules. For a pure (or almost pure) screw dislocation, its image is invisible when $\boldsymbol{g} \cdot \boldsymbol{b} = 0$. For a pure (or almost pure) edge dislocation, its image is invisible when $\boldsymbol{g} \cdot \boldsymbol{b} = 0$ and $\boldsymbol{g}$ is parallel (or nearly parallel) to the line direction $\boldsymbol{u}$. For the general case of a mixed dislocation, visibility is least when the conditions $\boldsymbol{g} \cdot \boldsymbol{b} = 0$ and $\boldsymbol{g} \times \boldsymbol{b} \cdot \boldsymbol{u} = 0$ are most nearly satisfied. The visibility plot, figure 5, explained in its caption, refers to the prominent array of glide dislocations lying in $(11\bar{1})$ that are seen in plan in the topographs, and whose Burgers vector is parallel to [011]. (The sign of the Burgers vector is undetermined.) Their images show features arising from interactions with dislocations belonging to slip systems on $(\bar{1}1\bar{1})$ and (111). The former interactions manifest themselves in the cusps, as seen mainly in the left part of the array. More notable are interactions with dislocations gliding on (111), which give rise to the straight-line segments parallel to $[\bar{1}10]$, horizontal in the topographs, e.g. in figure 4(*a*). Dislocations belonging to the $(\bar{1}1\bar{1})$, $[10\bar{1}]$ slip system are invisible in figure 4(*a*), but visible in figure 4(*b*). The horizontal, $[\bar{1}10]$-line-direction images seen in (*a*) disappear in (*b*). This (and other) evidence shows that they are pure edge segments, Burgers vector direction [110]. In figure 4(*c*) all images become vestigial (excluding those in the 'dark clouds' where long-range strains due to dislocation pile-ups have occurred). Nearly pure edge segments in the array due to $(11\bar{1})$, [011] slip are all but invisible; the pure edge segments parallel to $[\bar{1}10]$ with Burgers vector direction [110] are weakly visible. In figure 4(*d*) the latter dislocations stand out strongly. They have been formed through the Lomer reaction between $(11\bar{1})$ [011] glide dislocations and (111) $[10\bar{1}]$ glide dislocations. These have united to produce lines parallel to the intersection of the two slip planes concerned, but having the Burgers vector direction [110] which is contained in *neither* slip plane. Such dislocations are not glissile. In this and other specimens they can be seen as obstacles to glide, forming the core of dislocation tangles.

6. Expanding applications

A discussion with Professor Charles Frank at Bristol in August 1957 disclosed a common interest in diamonds and the likely dislocation configurations therein. In the winter of 1958–9 I visited Bristol, bringing my camera with me. X-ray topographs of dislocations in diamond (Frank and Lang 1959) and in strain-anneal-grown crystals of aluminium (Lang and Meyrick 1959) were then obtained. (Work on aluminium was later pursued with the help of André Authier (Authier *et al* 1965).) In the initial years of x-ray topographic studies of dislocations, I felt it important to study as wide a range of crystal species as possible, both to illustrate the versatility of a method based on the laws of x-ray diffraction that all good crystals obeyed, and to advertise the potential value to crystal growers of this non-destructive technique for assessing their products. Dates of publications of x-ray topographic experiments done first at Harvard and from 1960 onwards at Bristol do not usually indicate how early in the era of high-resolution x-ray topography the studies were performed, due to this author's dilatoriness in writing papers; and many studies have never been written up at all.

7. Breaking the rules: the failure of Friedel's law

When the first hkl, $\bar{h}\bar{k}\bar{l}$ stereo-pairs were recorded it was often observed that the diffuse, dynamical images of dislocations (either of individuals or of arrays) were unequally strong in the members of the pair, and indeed there could be excess intensity above background in the hkl image, say, and deficiency below background in $\bar{h}\bar{k}\bar{l}$. The effect was more pronounced the higher the x-ray absorption, and appeared to arise from long-range lattice curvature, as produced, for example, by dislocation pile-ups. I termed this phenomenon 'departure from Friedel's law' with regard to topographic images of crystal defects, but could muster no theoretical explanation.

In October 1960, Polder, Okkerse and Penning visited Bristol. Polder expounded to Mike Hart (who had just started his PhD research) and to me the concepts

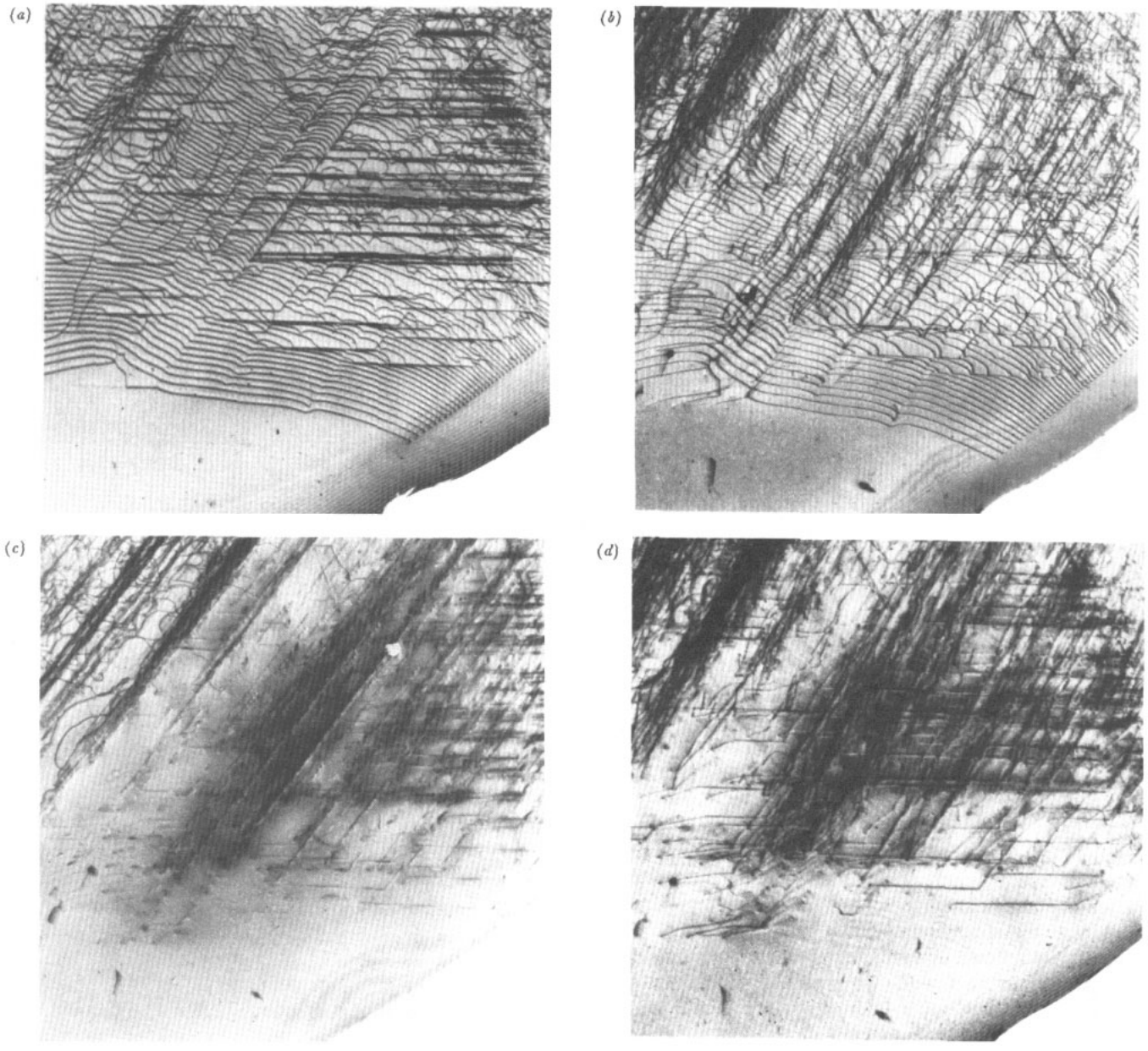

Figure 4. Projection topographs of part of $(11\bar{1})$ slice of silicon 1 mm thick, direction $[\bar{1}10]$ horizontal. Field width 6.25 mm. Radiation $AgK\alpha_1$. Diffraction vector directions shown in figure 5. Reflections: (*a*) $\bar{1}\bar{1}\bar{1}$; (*b*) $\bar{2}20$; (*c*) $1\bar{1}1$; (*d*) $1\bar{3}1$.

now so well known as 'Penning–Polder theory' (Penning and Polder 1961). Application of their principles of 'refraction of energy flow' under conditions of moderately strong x-ray absorption in order to show that x-ray topographs could determine the *sense* of dislocation Burgers vectors in addition to their orientation was a major theme in Hart's thesis work (Hart 1963). Into Ge and InSb crystals nearly dislocation free, fresh dislocations were introduced by carefully controlled plastic deformation in a three-point, bending jig held at the appropriate temperature. In the simple, single-slip systems produced, the geometrical conditions of the bending told one what the *sense* of every dislocation Burgers vector must be. Departure from Friedel's law showed up in two environments, at dislocation outcrops where elastic relaxation produced local lattice curvature, and in the diffuse image surrounding the core kinematic image of a dislocation that took its trajectory within the crystal. For both environments semi-quantitative developments of Penning–Polder theory were applied and agreed with experiment. Figure 6 illustrates a representative example of one of Hart's experiments done around 1962. It shows parts of topographs of a germanium slice prepared by Mike Hart so as to contain some of the dislocation half-loops he had deliberately introduced into the specimen bar. The dislocations are mainly of 60° character. In this pair of images one sees clearly demonstrated the contrast reversal oc-

curring when g is reversed. This applies to both the black–white lobes at dislocation outcrops, and to the diffuse component of images of dislocations threading the crystal.

8. Breaking the rules: determining relative phases

Determining relative phases of x-ray reflections from intensities measured under two-beam conditions is at the heart of x-ray crystallography. Finding relative phases of two (or possibly more) simultaneous reflections by study of the reflection intensity of one reflection is theoretically possible with perfect crystals when Umweganregung occurs. Doing the job without measuring *any* reflection intensity at all would be ruled impossible, according to conventional x-ray crystallographic thinking. But this rule was broken in 1961.

When setting up a crystal for topography, using reflection g, say, the crystal being perhaps 2 cm high and distant 50 cm from the x-ray source, the axial angle (over 2°) subtended by the crystal at the source would not infrequently straddle the Bragg condition for another reflection, g', with g' lying out of the plane normal to the goniometer axis. At the height on the specimen crystal where both g and g' satisfied Bragg's law, three-beam diffraction occurred (or n-beam, $n > 3$, under conditions of high symmetry). In consequence, an Aufhellung appeared in the image g. (The three-dimensional geometry is essentially that shown in figure 2 of Lang (1957b).) In the case of a projection topograph the Aufhellung would be drawn out into a horizontal line across the topograph, sometimes marring the image of a feature one wished to record. (Generally a small rotation of the specimen about g could be used to drive the g' Aufhellung upwards or downwards as desired.)

As part of his work on studying diffraction contrast as μt varied, Mike Hart developed techniques for producing Ge and InSb specimens with flat surfaces and thickness gently tapering to a wedge edge. Figure 7 is a topograph of a Ge wedge that contained a small population of long edge dislocations parallel to the [110]-type direction of the wedge edge. (In the thicker parts of the wedge, where Pendellösung fringes have disappeared due to dominance of Branch I waves, these dislocations show contrast reversal, appearing as deficiencies of intensity.) Of present interest is the Aufhellung running horizontally across the image, towards the upper corner of the wedge. Just above the Aufhellung, the Pendellösung fringe spacing is increased, and just below it is diminished, in consequence of the different distortions of the g dispersion surface on either side of exact satisfaction of both g and g' Bragg conditions. Many observations of this type were made.

Fortunately I knew about the Kambe–Miyake analysis of the three-beam case in electron diffraction (Kambe and Miyake 1954, Miyake and Kambe 1954), and saw that it could be easily applied to our x-ray experiments. Perhaps too easily! I recall a very uncomfortable day

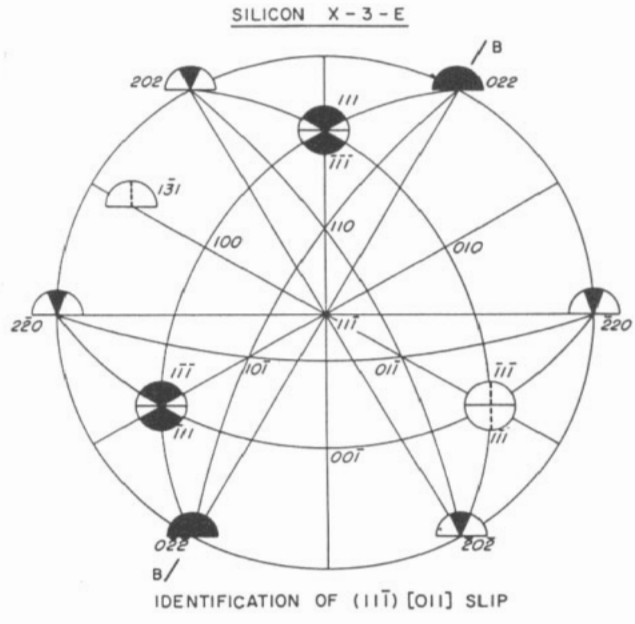

Figure 5. Visibility diagram for dislocations in the array belonging to the $(11\bar{1})$, [011] slip system seen in figure 4. Relative visibility indicated by angular width of black sector in the semicircle labelled with the reflection operating. Interrupted vertical radial line signifies trace visibility.

Figure 6. Dislocations of known sign of Burgers vector deliberately introduced into germanium specimen. Dislocation images showing contrast reversal when g is reversed, $\mu t \approx 3$.

when the contraction and expansion of Pendellösung fringe spacing I derived from their theory was in the opposite sense to that observed. Shortly I realized that I had forgotten to make the switch required in consequence of the mean refractive index for x-rays being *less* than unity, and then things came out all right (Hart and Lang 1961).

9. Magnetic domains

A brief but very fruitful visit by Milena Polcarová to Bristol in early 1962 had as its initial aim the study of dislocations within Fe + 3 wt% Si crystals grown in Prague. Several interesting observations were made on this topic, including examples of dislocations aggregating to form

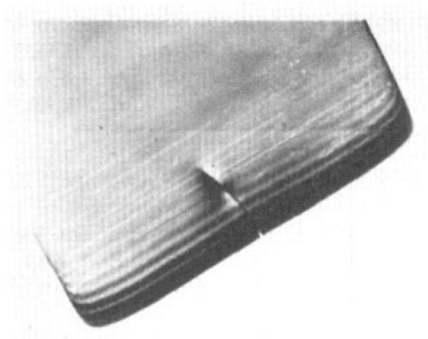

Figure 7. Aufhellung crossing topograph of a germanium wedge, one face parallel to (111). Symmetrical 220-type reflection, AgKα_1 radiation. Look along the Pendellösung fringes to observe the change in fringe spacing above and below the Aufhellung. (Disregard the accidental crack in the specimen half-way up the wedge edge.)

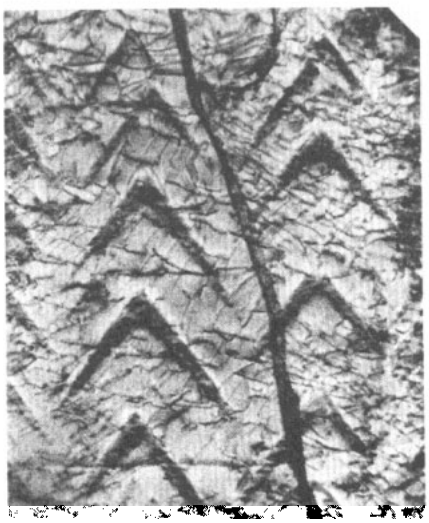

Figure 8. X-ray topograph revealing previously unobserved internal magnetic closure domain structures within a single-crystal (110)-orientation plate of iron–silicon alloy. Specimen mean thickness about 70 μm, tapering gently from top to bottom of image. Field width 1 mm, direction [001] vertical. Bragg reflection 002 in symmetrical transmission, AgKα_1 radiation. A low-angle boundary traverses the field from top to bottom, and dislocations are distributed over the field with density between 10^2 and 10^3 lines/mm^2. Of special interest are the chevron-shaped features that produce positive (dark) diffraction contrast. The vertical bisectors of the chevrons lie on 180° domain walls (invisible in this image) whose traces run vertically, parallel to [001], and which separate domains with magnetization directions [001] and [00$\bar{1}$] in the plane of the plate. The arms of these internal chevrons consist of a lamination of ±[100]- and ±[010]-magnetization-direction domains which carry flux between ±[001]-magnetization domains without formation of free magnetic charges internally or on the specimen surfaces.

low-angle boundaries (one of the happenings inside metal single crystals one had long wanted to investigate, as mentioned above in section 2). The dislocation observations were published some time later (Lang and Polcarová 1965). In single-crystal plates of iron–silicon alloy parallel to (110), Bitter patterns show 180° domain walls parallel to [001]. These lie between domains whose magnetization directions are respectively [001] and [00$\bar{1}$], say. Sometimes the Bitter pattern shows little kinks or indistinct segments in the wall, especially when the specimen tapers gently. The x-ray topographs revealed that at these loci there existed totally internal magnetic closure domain structures, of chevron-like outline, and composed of alternate [100] and [010] magnetization domains, perhaps 10 to 20 μm thick, that in combination could feed flux from a major [001] domain across to a major [00$\bar{1}$] domain without any free pole appearing at the surface. Many observations of these internal structures in tapering (110) plate specimens were made at Bristol in 1962 and following years, and to my disgrace have never been published. A pattern of 1962 vintage is shown in figure 8.

Strong x-ray diffraction contrast is generated at 90° domain walls in iron–silicon. These walls are coherent junctions of two crystals, which if free have very slight tetragonality in orthogonal directions. The effective misorientation (i.e. combination of tilt and interplanar spacing change) encountered by a Bragg-diffracted x-ray beam when crossing a 90° domain wall is in the general case only a few arc seconds. But this is comparable with the perfect-crystal angular range of reflection of shorter wavelengths such as MoKα and AgKα, and is ample for contrast generation by interbranch scattering across the dispersion surface. In plate specimens that do not contain a direction of easy magnetization, the whole volume is divided into a hierarchy of domains. This happens in the case of plates parallel to (112). Topographs showing contrast due to internal domain structures with this specimen geometry were used to exemplify the capability of the x-ray method for detecting domain structures and their movements (Polcarová and Lang 1962).

10. Concluding note

The final epoch in the five years spanned in this history saw a distinguished couple working in Bristol, Satio Takagi and his wife Meiko Takagi. Husband Takagi was busy deriving his well known 'Takagi equations' for dealing with distorted crystals (Takagi 1962), and Meiko developed diffuse-reflection topography (Takagi and Lang 1964). Our diffuse-reflection topographs of diamonds required exposure times up to 90 hours! Synchrotron x-rays were not available in those far-off days.

References

Authier A, Rogers C B and Lang A R 1965 *Phil. Mag.* **12** 547–60

Bond W L and Andrus J 1952 *Am. Mineral.* **37** 622–32

Bonse U and Kappler E 1958 *Z. Naturf.* **13a** 348–9

Borrmann G, Hartwig W and Irmler H 1958 *Z. Naturf.* **13a** 423–5

Chalmers B 1964 *Principles of Solidification* (New York: Wiley)

Ewald P P 1933 *Handbuch der Physik* **23** Bd 2 207–476

Frank F C and Lang A R 1959 *Phil. Mag.* **4** 383–4

Guinier A and Tennevin J 1949 *Acta Crystallogr.* **2** 133–8

Hart M 1963 *PhD Thesis* University of Bristol
Hart M and Lang A R 1961 *Phys. Rev. Lett.* **7** 120–1
Hirsch P B 1952 *Acta Crystallogr.* **5** 176–81
Hirsch P B and Ramachandran G N 1950 *Acta Crystallogr.* **3** 187–94
Jenkinson A E and Lang A R 1962 *Direct Observations of Imperfections in Crystals* ed J B Newkirk and J H Wernick (New York: Interscience) pp 471–95
Kambe K and Miyake S 1954 *Acta Crystallogr.* **7** 218–9
Kato N 1992 *P P Ewald and his Dynamical Theory of X-ray Diffraction. A Memorial Volume for Paul Ewald, 23 January 1888–22 August 1985* ed D W J Cruickshank *et al* (Oxford: Oxford University Press/IUCr) ch 1
Kato N and Lang A R 1959 *Acta Crystallogr.* **12** 787–94
Lang A R 1957a *Acta Metall.* **5** 358–64
—— 1957b *Acta Crystallogr.* **10** 252–4
—— 1957c *Acta Crystallogr.* **10** 839
—— 1958 *J. Appl. Phys.* **29** 597–8
—— 1959 *Acta Crystallogr.* **12** 249–50
—— 1992 *International Tables for Crystallography* vol C ed A J C Wilson (Dordrecht: Kluwer) pp 113–23
Lang A R and Meyrick G 1959 *Phil. Mag.* **4** 878–80
Lang A R and Polcarová M 1965 *Proc. R. Soc.* A **285** 297–311
Lomer W M 1951 *Phil. Mag.* **42** 1327–31
Miyake S and Kambe K 1954 *Acta Crystallogr.* **7** 220
Newkirk J B 1958 *Phys. Rev.* **110** 1465–6
Penning P and Polder D 1961 *Philips Res. Rep.* **16** 419–40
Polcarová M and Lang A R 1962 *Appl. Phys. Lett.* **1** 13–15
Ramachandran G N 1944 *Proc. Indian Acad. Sci. Sect. A* **19** 280–92
Takagi M and Lang A R 1964 *Proc. R. Soc.* A **281** 310–22
Takagi S 1962 *Acta Crystallogr.* **15** 1311–12
Uyeda R 1981 *Fifty Years of Electron Diffraction* ed P Goodman (Dordrecht: Reidel) pp 123–35
Wooster N and Wooster W A 1945 *Nature* **155** 786–7